Solid-state foaming of titanium by superplastic expansion of argon-filled pores

N.G. Davis, J. Teisen,[a] C. Schuh, and D.C. Dunand
Department of Materials Science and Engineering, Northwestern University, Evanston, Illinois 60208

(Received 5 January 2001; accepted 5 March 2001)

Solid-state foaming of commercial purity titanium was achieved by hot-isostatic pressing of titanium powders in the presence of argon, followed by expansion of the resulting high-pressure argon bubbles at ambient pressure and elevated temperature. The foaming step was performed under isothermal conditions or during thermal cycling around the α/β allotropic temperature of titanium. Such thermal cycling is known to induce transformation superplasticity (TSP) in bulk titanium due to the complex superposition of internal transformation stresses and an external biasing stress; TSP was found to be active during foaming, where the deviatoric biasing stress was provided by the internal pore pressure. As compared to isothermal control experiments where foam expansion occurred by creep only, TSP foaming under thermal cycling conditions led to significantly higher terminal porosity (41% as compared to 27%). The foaming rates were also higher for the TSP case before pore growth ceased. Additionally, foaming experiments were conducted under an externally applied uniaxial tensile stress of 1 MPa. This procedure resulted in foaming kinetics and porosities similar to those achieved without an external stress and, for the TSP case, led to high aspect ratio pores elongated in the direction of the applied external stress.

I. INTRODUCTION

Titanium-based foams have many potential applications due to titanium's outstanding mechanical properties, low density, and high chemical resistance. Potential uses include load-bearing applications as sandwich cores in the aerospace and ship-building industries[1,2] and as porous implants in the biomedical industry, for which the excellent biocompatibility and fatigue properties of titanium are also essential.[1–5]

Several different methods exist for metallic foam fabrication, as reviewed in Refs. 1 and 2. Some metallic foam can be formed in the melt, e.g., by adding foaming agents (gas or gas-producing solids) during solidification, by lost-foam casting, by infiltration of a granular bed, or by gas-eutectic transformation.[1,2] While these techniques have been commercially successful in fabricating, e.g., aluminum and zinc foam,[1,2] they are unsuitable for foaming titanium and titanium alloys due to the high melting temperature and melt reactivity of titanium. Furthermore, sintering of loose powders gives only low porosities (except when a fugitive filler is used[6]) while sintering of short wires is uneconomical for titanium. Slurry foaming, electrolytic deposition, and metal sputtering on a polymer substrate are also unsuitable for titanium foams due to contamination from the polymer substrate during its removal by burn-off. Solid-state foaming methods are thus more promising options for titanium foam production.

A novel technique for solid-state processing of Ti–6Al–4V foams was first described and patented by Kearns *et al.*,[7–9] and later by Martin,[10] and also investigated by Schwartz *et al.*[11] and Dunand and Teisen[12] (who also studied foaming of unalloyed titanium). The process is schematically depicted in Fig. 1. High-pressure argon bubbles are created in a metallic matrix by hot isostatic pressing (HIPing) metal powders in the presence of argon gas. The resulting material exhibits low pore fractions (typically less than 1%) composed of numerous micron-sized high-pressure argon pores. On annealing at ambient pressure and elevated temperatures, the high-pressure gas causes the bubbles to expand by creep of the surrounding metal. Kearns *et al.*[7–9] reported porosities of up to approximately 40% after heat treatments at very high temperatures (1250 °C) and long hold times (several days). The growth rate of the pores was controlled by the slow creep deformation of the metal.

Additionally, it has been shown that the HIPed material could be rolled or extruded prior to isothermal foaming.[7–11,13] The argon-filled pores were elongated during hot-working, and the subsequent foaming expansion was

[a]Present address: Medtronic AVE, 2345 Circadian Way, Santa Rosa, CA 95407.

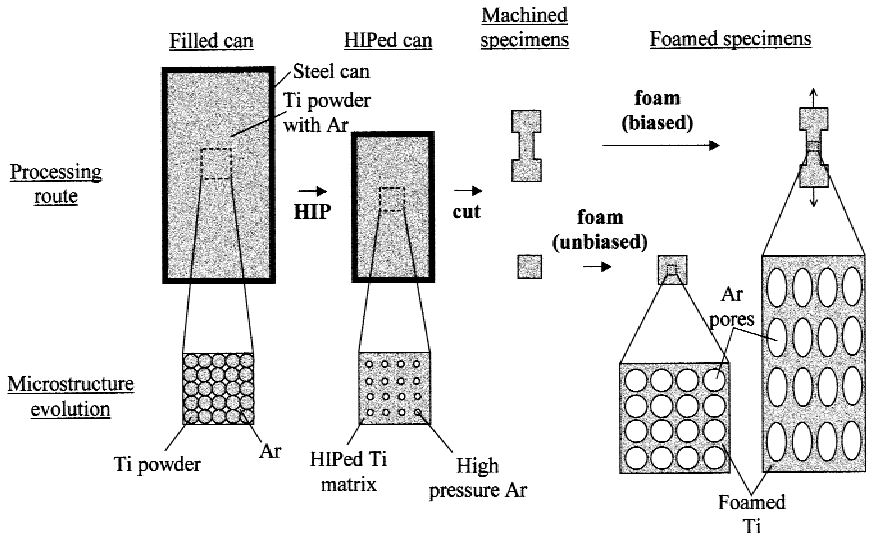

FIG. 1. Schematic of foaming process, where metal powders are first compacted in the presence of argon and the resulting high-pressure argon bubbles are then expanded under biased or unbiased conditions.

found to be anisotropic, with the least amount of expansion taking place in the direction of rolling or extrusion.[7–10,13] The resulting foam had pores that were partially aligned in the rolling direction, and the pore aspect ratio distribution had narrowed during foaming.[13]

Isothermal foaming occurs by creep of the matrix, which is associated with low deformation rates and, hence, slow foaming kinetics and modest porosities. A possible solution to these limitations is to use superplastic titanium, which deforms rapidly at low stresses and exhibits very large tensile ductility under uni- and multiaxial stress conditions.[14] Thus, foaming titanium under superplastic conditions could lead to faster foaming rates and higher terminal porosities. Typically, superplasticity occurs by grain-boundary sliding in metals with fine grains (<10 μm).[14] This so-called microstructural superplasticity cannot be achieved in unalloyed titanium because of rapid grain growth to sizes above the critical value of 10 μm, but is easily achievable in Ti–6Al–4V because its duplex structure inhibits grain growth. However, the fine grain size necessary for microstructural superplasticity in bulk Ti–6Al–4V is achieved by complex thermomechanical treatments (e.g., rolling and annealing).[14] As-HIPed Ti–6Al–4V is thus typically incapable of superplastic deformation without subsequent thermomechanical treatment. Such treatments are possible on the as-HIPed preform[7–10,13] but increase costs and significantly change the pore morphology as pores elongate and link during rolling, possibly limiting the subsequent pore expansion.

An alternate superplastic mechanism in polymorphic materials such as commercial purity Ti (CP–Ti) and Ti–6Al–4V is transformation superplasticity (TSP) as Dunand and Teisen[12] demonstrated for foams of CP–Ti and Ti–6Al–4V. Because this type of superplasticity has no minimum grain size requirement, it is applicable to both CP–Ti and Ti–6Al–4V immediately after powder compaction and without any thermomechanical treatments. TSP has been reported in fully dense titanium,[15–21] Ti–6Al–4V,[18,20,22–25] and many other polymorphic metals, alloys, and metal–matrix composites, as reviewed in Refs. 14 and 26.

The mechanism for TSP relies on internal mismatch strains produced by the density difference between the two allotropic phases coexisting during the phase transformation. These mismatch strains are biased in the direction of an externally applied stress, resulting in a net strain increment in the biasing direction accumulated during the phase transformation. By multiple cycling through the phase transformation, these strain increments can be accumulated to elongations well in excess of 100% without fracture or cavitation.

In this paper we investigate foaming of CP–Ti under TSP conditions, using the internal gas pressure of the pores as the biasing stress, and thermal cycling to induce transformation mismatch. We compare final porosities and foaming rates with the original isothermal process of Kearns *et al.*,[7–9] where deformation occurs solely by creep. We also explore the effect of an externally applied uniaxial tensile biasing stress on foaming rates, final porosities, and pore morphology.

II. EXPERIMENTAL PROCEDURES

Spherical CP–Ti powders (−100 mesh size, Grade II, from Starmet, Concord, MA) with median size of approximately 130 μm were used. The powders contained 0.14 wt% O and Fe, 0.01 wt% N and C, and <0.01 wt% H. Specimen preparation is depicted schematically in Fig. 1. Powders were packed to approximately 70% density by applying uniaxial pressure at room temperature in

a steel can, which was evacuated, back-filled with 0.33 MPa of Ar, and sealed. The canned powders and Ar were densified by HIPing at 890 °C and 100 MPa for 125 min at UltraClad (Andover, MA).

A. Unbiased foaming experiments

Cubic specimens with approximately 6-mm edges were cut from the HIPed billets by electrodischarge machining and lightly polished with 600 grit SiC paper. These specimens were then foamed either by thermal cycling or by isothermal anneal. Thermal cycling was performed on specimens encapsulated in quartz tubes (which were evacuated to 0.01 mtorr) together with a tantalum gettering foil, or on nonencapsulated specimens within a vacuum furnace evacuated to 10–30 mtorr residual argon atmosphere. Despite being placed within a thin titanium foil getter cage, the latter specimens exhibited a thin black surface layer, which was found by x-ray diffraction to be titanium carbide and dioxide resulting from residual contaminants and degassing from graphite heating elements. A separate as-HIPed specimen was used for each unbiased foaming experiment performed under thermal cycling or isothermal conditions.

For the superplastic foaming experiments, specimens were thermally cycled between 830 and 980 °C, spanning the allotropic temperature range of CP–Ti (nominally at 882 °C, but expected to be higher and wider due to the oxygen content[27,28]) with a 4-min cycle period. These experiments had a total duration of 30 min to 24 h.

In creep-foaming experiments, vacuum-encapsulated specimens were introduced in a preheated furnace and rapidly heated to the isothermal temperature of 903 or 960 °C. Total annealing times were from 8 min to 24 h, followed by water quenching. The higher temperature of 960 °C was close to the upper temperature used in the cycling experiments (980 °C) and well within the β-field of CP–Ti. The lower temperature of 903 °C corresponds to the effective temperature of the thermal cycle described above; the effective temperature is defined as the temperature at which the isothermal creep rate is the same as the time-averaged creep rate during thermal cycling in the absence of TSP[17,22] found by using lattice activation energies given in Ref. 29 for α–Ti and β–Ti. Thus, any enhancement in the thermal cycling foaming kinetics as compared to those at the effective temperature (903 °C in the present case), can be attributed to the effect of TSP on foaming.

B. Foaming with an external tensile biasing stress

In addition to the above cubic specimens, two 20-mm-long cylindrical tensile specimens were machined with an 8-mm gauge length and with gauge and head diameters of 4 and 9 mm, respectively. Each specimen was then foamed in a custom-built tensile creep frame (described in Ref. 30) under an inert argon atmosphere at 1 atm while being subjected to an externally applied uniaxial biasing stress. The uniaxial tensile load, F, was adjusted such that the average stress acting on the titanium matrix (approximated as $F/A(1-f)$, where f is the pore fraction and A is the instantaneous cross-sectional area) was constant at 0.98 ± 0.08 MPa (referred to simply as 1.0 MPa hereafter). In the above approximation, any stress concentrations due to the presence of porosity has been neglected. In addition, these experiments were interrupted seven times by excursions to room temperature to determine gauge porosity and instantaneous cross-sectional area (by measurement of the gauge section dimensions) and to adjust the load to maintain the net uniaxial biasing stress of 1.0 MPa.

C. Foam characterization

After foaming, density measurements were performed by the Archimedes method in distilled water on all specimens foamed under unbiased conditions as well as on the sectioned gauge of the specimens foamed with a biasing stress. The surface of each specimen was sealed with a thin layer of vacuum grease to prevent water infiltration of open porosity, thus yielding direct measurement of the total porosity (sum of open and closed porosity). The error in density measured by the Archimedes method was estimated as ± 0.0038 g/cm^3 ($\pm 0.1\%$ porosity). The surface of the unencapsulated specimens foamed without a uniaxial biasing stress were lightly polished to remove contamination prior to measurement. For select unbiased specimens and for the gauge of the specimens foamed under an external biasing stress, density (and, thus, total porosity) was also determined by dimensional measurements. Density from these measurements was found to be very close to the density determined by the Archimedes method, indicating that both methods give reliable values of the total porosity. Also, density measurements were performed using helium pycnometry (AccuPyc 1330, Micromeritics, Norcross, GA) on some specimens. Since helium gas can readily infiltrate porosity open to the surface, the volume measurements by this technique assess only closed porosity in the foam.

Selected specimens were metallographically prepared by grinding and polishing to 0.05 μm. To minimize pore wall deformation during metallographic preparation, the porous specimens were vacuum-infiltrated with epoxy resin at regular intervals during polishing, which filled the pores connected to the surface. Some specimens were etched by a modified version of Kroll's reagent (10% HF, 5% HNO_3, and 85% H_2O). Optical micrographs were used to find the longest pore dimension as well as the maximum pore dimension perpendicular to it, from which the pore aspect ratio was calculated.[31]

Representative foams produced both with and without a biasing stress were tested in uniaxial compression at room temperature using a screw-driven load frame. Compression specimens were machined into parallelepipeds with a height to width ratio of 1.75 for the isothermal specimens and 2 for the thermally cycled foams. For the specimens foamed with a biasing stress, the compression axis was the same as the axis of the tensile loading used during the foaming procedure. A laser extensometer was used to measure compression platen displacement. In addition, elastic constants of isothermal and thermally cycled unbiased foams foamed for 11.8 h were found nondestructively by the ultrasonic pulse echo method[32–34] using a digital oscilloscope with 5 and 2.25 MHz transducers.

III. RESULTS

As shown in Fig. 2, initial pores in the HIPed billets retained the general shape of the gap between powders in the original preforms and were thus nonspherical, as also reported in Refs. 7–9 for Ti–6Al–4V HIPed at 100 MPa and 950 °C for 4 h with backfill pressures of up to 0.05 MPa. Initial average pore size was roughly 25 μm, and the initial porosity was about 0.55%. Matrix grain size was about 50 μm, much larger than the critical value of 10 μm above which structural superplasticity is inactive.

A. Unbiased foaming

The average specimen porosity as a function of annealing time for unbiased foaming is shown in Fig. 3 under isothermal conditions (at 903 and 960 °C) and under cyclic conditions (830 to 980 °C). Thermal cycling results in the fastest rate of foaming and the highest terminal porosity after 24 h (41% for thermal cycling, as compared to 26% or 27% for isothermal experiments at 903 and 960 °C, respectively). No significant difference in foaming kinetics was noted between the encapsulated and the nonencapsulated specimens. Both isothermal and thermally cycled specimens foamed for 11.8 h had only small amounts of open porosity, as observed by the difference between the total and closed porosity: an eighth of the total porosity was open to the surface for the isothermally foamed specimen (960 °C) while a tenth of the total porosity was open for the thermally cycled foam. Reproducibility was tested by foaming three specimens at 903 °C for 24 h yielding similar porosities for each specimen: 26%; 22%; 21%. Since foaming kinetics and achievable pore fractions are dependent on the initial pore fraction (which can vary slightly with position in the HIPed canister due to powder settling), the reported amount of variation is considered reasonable.

Figure 4 shows the pore structure in CP–Ti after foaming under unbiased conditions for 5.25 h under isothermal creep conditions at 960 °C [Fig. 4(a)] and for 5 h under thermal cycling superplastic conditions [Fig. 4(b)]. In both cases, pores are rounded and have a diameter of up to 200 μm (many of the smaller pores result from the metallographic plane intersecting far from the equatorial plane of the roughly spherical pore). Pore coalescence is much more pronounced in the isothermally foamed specimen [arrows in Fig. 4(a)] than in the thermally cycled specimen, which exhibits many examples of very thin pore walls; many walls are less than 10 μm in thickness [arrows in Fig. 4(b)]. The etched matrix shows colonies of serrated α grains typical of CP–Ti annealed in the β field.[35]

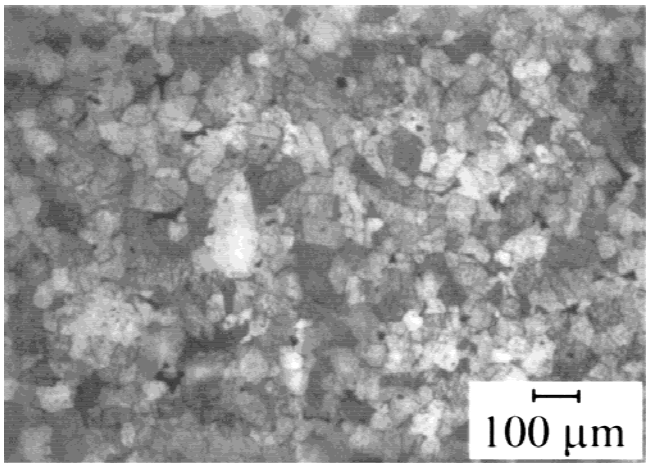

(a)

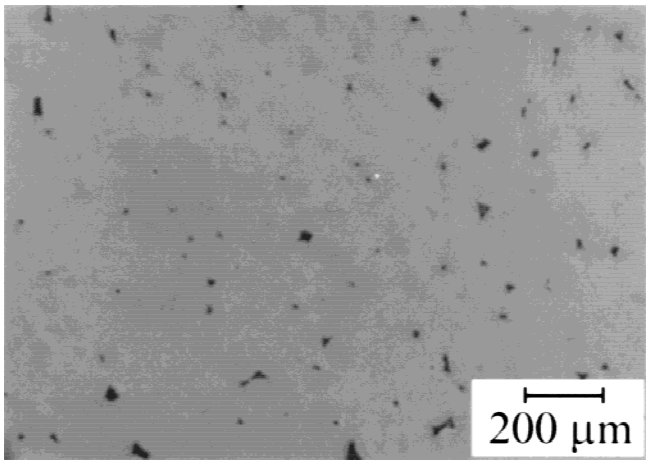

(b)

FIG. 2. Optical micrographs of as-HIPed CP–Ti: irregularly shaped Ar-filled pores at interstices of (nonvisible) prior powder particles with (a) etched matrix showing the grain structure and (b) unetched matrix showing the pore structure.

B. Foaming with an external stress

Figure 5(a) shows the gauge porosity as a function of foaming time for specimens foamed with a net external stress of 1.0 MPa for thermal cycling between 830 and

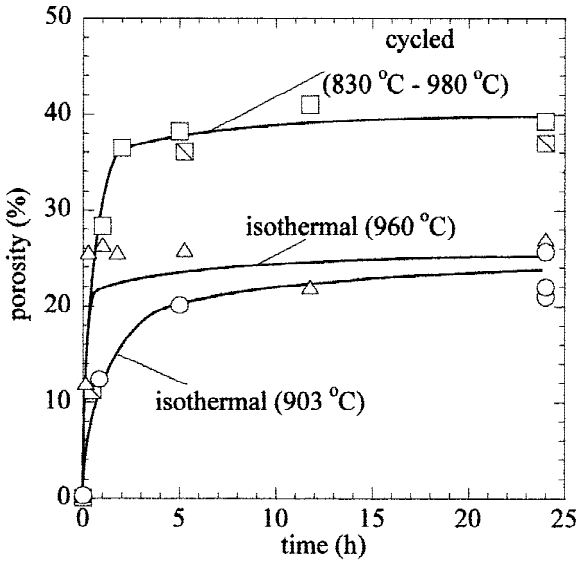

FIG. 3. Porosity as a function of time for isothermal and cyclic experiments for CP–Ti foamed without an external stress. Crossed symbols correspond to encapsulated, thermally cycled specimens.

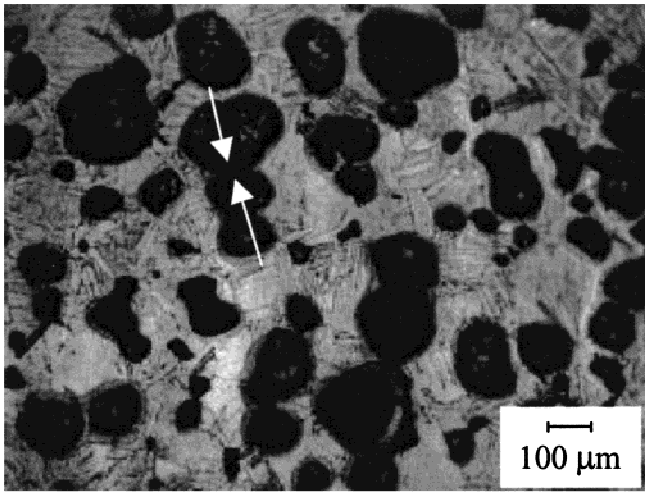

(a)

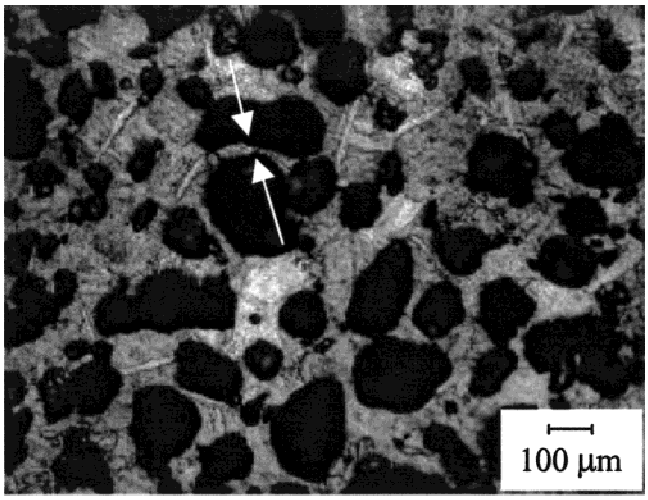

(b)

FIG. 4. Optical micrographs of CP–Ti foamed with no external stress (a) isothermally at 960 °C for 5.25 h with 27% porosity and (b) by thermal cycling between 830 and 980 °C for 5 h with 39% porosity. Arrows in (a) show pore coalescence with no evidence of thin, interpore regions while in (b) they show a thin interpore wall and much less pore coalescence.

980 °C and for isothermal foaming at the effective temperature of the thermal cycle, 903 °C. Following fracture of the cycled specimen after 11.8 h, the total gauge porosity was measured as 48%. After the material in the immediate vicinity of the fracture surface was removed, the total gauge porosity was found to be 41%. Thus, a significant amount of porosity developed near the site of fracture and is not representative of most of the specimen gauge. With the fracture surface removed, the gauge porosity is the same as that found in foams made by thermal cycling without a biasing stress for 11.8 h (Fig. 3). For the isothermal biased specimen, the gauge porosity after 11.8 h of foaming at 903 °C was found to be 20% and is also very close to the total porosity found for unbiased, isothermal foaming for 11.8 h at 960 °C (Fig. 3). A small amount of open porosity was found in the biased, isothermally foamed specimen while the thermally cycled specimen was found to have mostly open porosity: a fifth of the total porosity was open in the isothermal case compared with nine-tenths for the thermally cycled foam. Figure 6 summarizes the open and closed porosities for all specimens subjected to thermal cycling or isothermal foaming for 11.8 h.

Figure 5(b) shows the uniaxial gauge elongation (in the direction of the applied stress) as a function of foaming time for the biased specimens. The engineering fracture strain for the cycled specimen was 115%, as compared to 20% gauge elongation for the isothermal specimen after the same length of time.

In Figure 7, the microstructures from the externally stressed foamed specimens are shown. Figures 7(a) and 7(b) show, respectively, longitudinal and transverse sections, for the isothermal biased foaming (20% uniaxial strain, 20% porosity), exhibiting rounded pores with a maximum diameter of about 250 μm and some pore coalescence. Overall, the pores appear isotropic with no preferential alignment or elongation (except where pores have merged). Figures 7(c) and 7(d) show sections for the corresponding thermally cycled specimen (115% uniaxial strain, 41% porosity). The pores in Fig. 7(c) are notably elongated, with an average pore aspect ratio of 1.9 and a maximum aspect ratio of 5.0. Additionally, the pores are generally aligned in the direction of the applied stress and have maximum pore length of almost 1 mm. There is no notable pore alignment in the plane perpendicular to the applied stress.

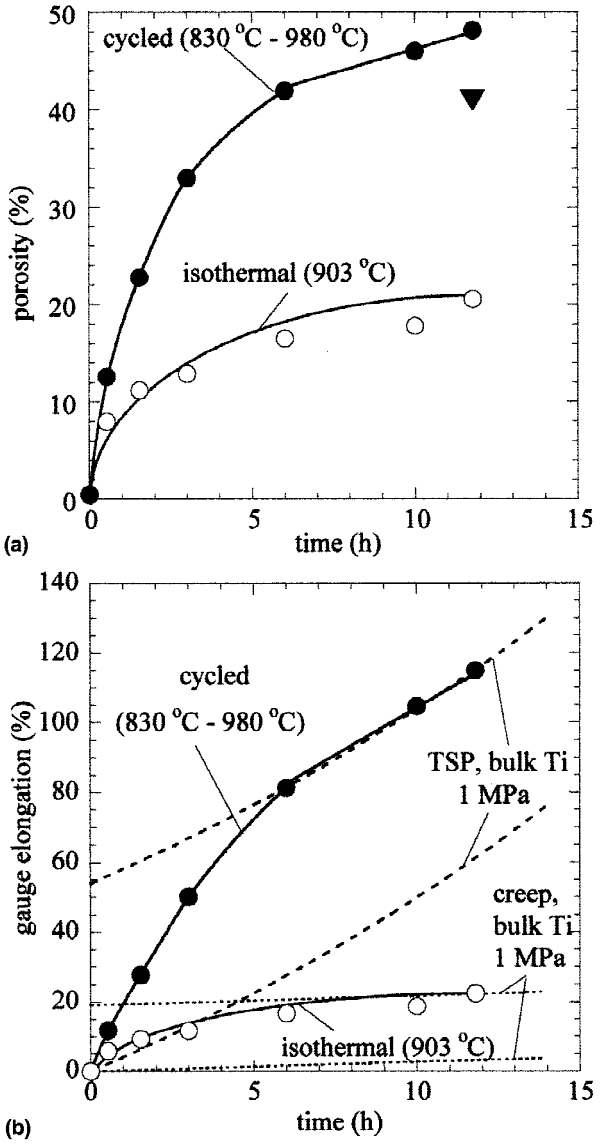

FIG. 5. Time dependence of (a) gauge porosity and (b) gauge elongation for CP–Ti foamed under isothermal and cyclic conditions with a superimposed external tensile stress of 1.0 MPa. The triangle in (a) is gauge density without material near fracture surface. The dotted line in (b) is the gauge elongation expected for creep of bulk Ti at 903 °C from Ref. 29, and the dashed line in (b) is gauge elongation for TSP of bulk titanium from Ref. 20. These lines are offset for comparison to foaming data.

C. Unbiased and biased foam mechanical properties

Figure 8 shows the room-temperature compressive stress–strain behavior of isothermal and thermally cycled foams processed for 11.8 h with and without an external tensile stress. Young's moduli for all specimens were found from the stress–strain curves to be roughly 40 GPa with a large error of ±20 GPa. The onset of yield for the isothermal foams (20–22% porosity) was about

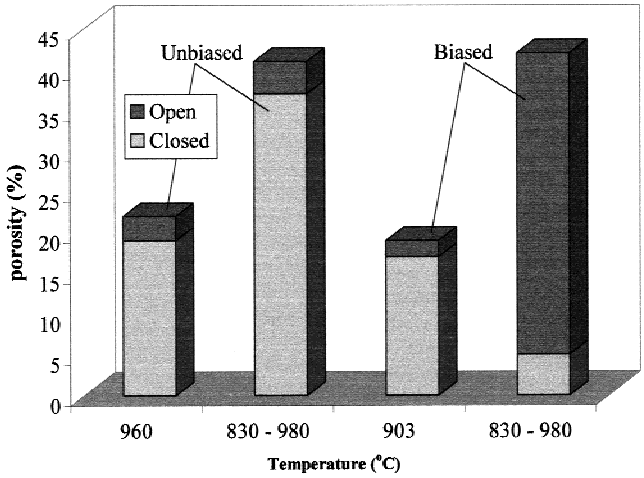

FIG. 6. Values of open and closed porosities for unbiased and biased foams foamed under isothermal or thermal cycling conditions for 11.8 h.

200 MPa, as compared to about 120 MPa for the thermally cycled foams (41% porosity), again with a large error of ±20 MPa.

Ultrasonic evaluation of the elastic constants for the unbiased specimens foamed for 11.8 h yielded Young's moduli of 60 and 39 GPa for isothermal anneal (960 °C, 22% porosity) and thermal cycling (41% porosity), respectively.

IV. DISCUSSION

A. Unbiased foaming

1. Isothermal foam production

While isothermal experiments by Kearns *et al.*[7–9] resulted in terminal porosities for Ti–6Al–4V higher than for our isothermal experiments for CP–Ti (32% versus 27%), there are four main differences between that study and the current investigation: alloy composition, backfill pressure, foaming temperature and foaming time (see Table I). Their specimens were annealed much longer (46 h versus 24 h) and at much higher temperatures (1240 °C versus 960 °C). However, in the present study, higher initial argon pressures were used (0.33 MPa versus 0.01 MPa) and a less creep resistant material was used (CP–Ti versus Ti–6Al–4V). With the first two parameters favoring higher porosities in their study and the last two in our study, it is difficult to directly compare the respective porosities.

2. Effect of thermal cycling on foam production

If one neglects the small pressure variation of ±6% due to thermal cycling, TSP cycling experiments can be compared directly to isothermal creep experiments carried out at the effective temperature. Figure 3 shows that the overall foaming rate is significantly higher under TSP

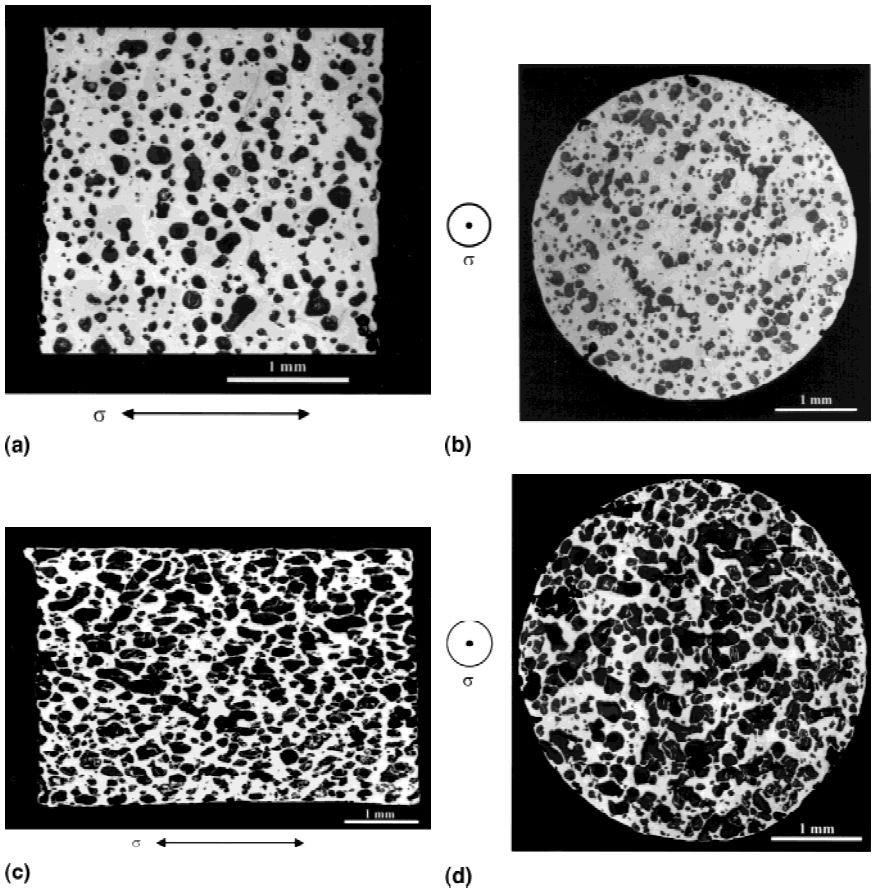

FIG. 7. Composite micrographs of specimens foamed under biased conditions for 11.8 h: (a, b) specimens with porosity of 20% foamed isothermally at 903 °C; (c, d) specimens with 41% porosity, thermally cycled between 830 and 980 °C. The direction of applied stress is shown.

conditions (830–980 °C) than under creep conditions at the corresponding effective temperature (903 °C). Furthermore, the terminal porosity is also much higher for the cycled specimens. This demonstrates that foaming under TSP conditions leads to both faster deformation rates and larger strains to fracture of the pore walls than under creep conditions, as is also observed for bulk CP–Ti and Ti–6Al–4V subjected to uniaxial and multiaxial tests.[18,22,23] Even when the cycling experiments are compared to isothermal experiments at 960 °C (well above the effective temperature and near the maximum cycling temperature of 980 °C), terminal total porosities are higher for the cycled specimens. In other materials, if no allotropic transformation exists, foaming enhancement due to internal mismatch strains may be induced in other ways, e.g., by thermal cycling in nonallotropic composites has shown deformation enhancement due to the difference in the thermal expansion between matrix and reinforcing phases as demonstrated for the case of uniaxial deformation.[14]

As seen in Figure 3, the foaming process reaches a plateau, after which there is no appreciable change in porosity. The time required to reach final porosity for unbiased, isothermal and cyclic foaming is summarized in Table I. In addition, the time to reach final pore fractions reported by Kearns *et al.*[7–9] and Queheillalt *et al.*[13] for Ti–6Al–4V are presented for comparison. In the present study, time to reach final porosity is shortest for isothermal foaming at 960 °C (0.5 h) and slowest for foaming isothermally at 903 °C (5 h), with cyclic foaming being intermediate (2 h). The average foaming rate, calculated as the ratio of the final porosity to the corresponding time, is roughly 1 order of magnitude slower at 903 °C than for thermal cycling. For foaming at 960 °C, the foaming rate was found to be roughly half an order of magnitude faster than for cyclic foaming but the terminal porosity was much lower.

A foaming body can be modeled as a series of small pressure vessels. The pressurized argon within each pore causes deformation of the surrounding material just as gas in a pressure vessel produces creep deformation of the vessel at elevated temperatures, a problem which is described by Finnie and Heller.[36] The simplest modeling approach for the foam is to consider equisized pores on a cubic lattice. A pore and the associated matrix can be equated to a spherical shell of inner and outer radii a and b, respectively. The deformation of a spherical pressure vessel[36] with $(a/b)^{1/3} = f$ is then a fair approximation

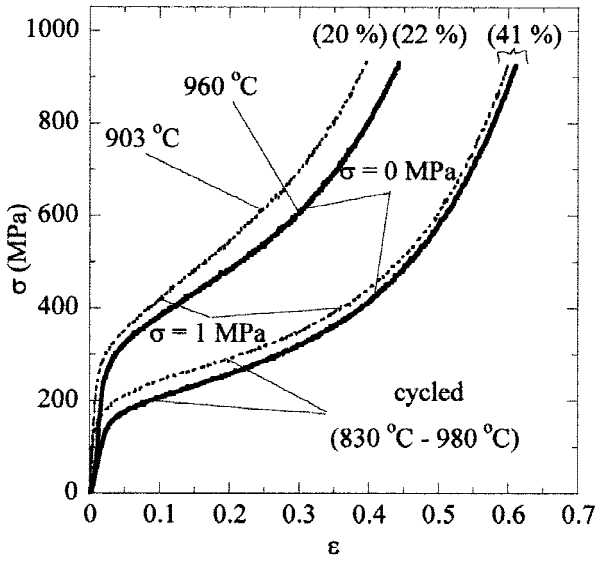

FIG. 8. Stress–strain curves (room-temperature compression) for CP–Ti specimens foamed for 11.8 h under isothermal and thermally cycled, biased (dotted curves) and unbiased (solid curves) conditions. Porosities are given in parentheses.

of the deformation of the foam. For this geometry, the average von Mises equivalent strain in the spherical shell, $\bar{\epsilon}$, is

$$\bar{\epsilon} = |\bar{\epsilon}_S| \quad , \tag{1}$$

where $\bar{\epsilon}_S$ is the average thickness strain in Eq. (1) defined as

$$\bar{\epsilon}_S = \ln\left(\frac{b_f - a_f}{b_i - a_i}\right) \quad . \tag{2}$$

Subscripts f and i are for the final (low pressure) and initial (high pressure) conditions. Using mass conservation and the experimentally measured initial and final porosities to find the initial and final average thickness strains, Eqs. (1) and (2) then predict that the average equivalent strain in the pore walls after foaming exhaustion is 0.6 and 1.0 for isothermal foaming at 903 °C and for cyclic foaming between 830 and 980 °C, respectively. This result suggests that superplastic strains have been achieved for thermally cycled foams and that superplastic deformation of the cell walls is responsible for the significantly larger overall pore size and porosity as compared to isothermal creep conditions. Additionally, due to the lower tensile ductility of CP–Ti under creep conditions than under TSP conditions, more pore coalescence is expected in the isothermal specimens than for the thermally cycled specimens. This is, indeed, confirmed by the observation that pore-wall rupture is more extensive in the isothermal specimens [arrows in Fig. 4(a)], while the superplastic specimen shows many more intact pore walls despite exhibiting pore fractions higher by a factor of 2. In the unbiased case, the fraction of open porosity is larger in the isothermal specimen than in the thermally cycled specimen (Fig. 6), suggesting an increased amount of pore coalescence.

3. Foaming saturation

At the onset of foaming, the gas pressure inside the pore and the stresses in the matrix are high and foaming, for all specimens, is dominated by creep of the pore walls. In later stages of foaming, as the pore pressure decreases with increasing pore size, the stress on the matrix is reduced and TSP becomes the dominant deformation mechanism for thermally cycled specimens. Since the effective temperature of the thermal cycle is 903 °C, it is not surprising that the foaming rate for the thermally cycled foam is slower than those foamed at 960 °C during the initial stage of foaming, before the deformation mechanism transition. In addition, CP–Ti annealed isothermally cannot foam by creep to the same extent as the thermally cycled foams, which are superplastic. Since TSP remains dominant at low stresses, pore growth continues in the cycled specimens in spite of the smaller pore pressures, allowing for further increase in porosity even when compared to a temperature close to the upper temperature of the thermal cycle.

This line of reasoning is further substantiated by the small fractions of open porosity found in either the isothermal or the thermally cycled cases (Fig. 6), suggesting that foaming cessation cannot solely be due to escape of the gas from pore wall bursting. Some open porosity was present in both isothermal and thermally cycled specimens foamed for 11.8 h. However, in both cases, less than an eighth of the total pore fraction was open to the surface (Fig. 6). Any pores open to the surface are no longer available for further foaming, as the gas has escaped, removing the driving force for foaming. Effects reducing the total achievable porosity by promoting pore coalescence include limited tensile ductility, nonuniform spatial and size distribution of pores (dictated by the powder size distribution), and nonspherical pore shapes. Additionally, friction between the specimen's supporting surface and external specimen surfaces (which were indeed found to become rough as a result of individual pore bulging at the surface) can limit the total achievable porosity.

Mass conservation gives the maximum final porosity f_f achievable after complete foaming as

$$f_f = \frac{s}{s + f_o^{-1} - 1} \quad , \tag{3}$$

where $s = p_o T_f / p_f T_o$ is the ratio of the pore volumes (according to the ideal gas law) after foaming and before HIPing, with p and T the pressure and temperature. Using the present experimental conditions ($f_o = 0.3$, $p_o = 0.33$ MPa, and $T_o/T_f = 300/1233$) and noting that a

TABLE I. Comparison of maximal porosities and average foaming rates for unbiased foams for this and previous studies.

	Present study			Kearns *et al.*[7–9,a]	Queheillalt *et al.*[13]
Material	CP–Ti	CP–Ti	CP–Ti	Ti–6Al–4V	Ti–6Al–4V
Thermal conditions	903 °C	960 °C	830–980 °C	1240 °C	920 °C
Backfill pressure (MPa)	0.33	0.33	0.33	0.01	0.3
Max. porosity (%)	22	27	41	32	22[b]
Time to reach max. porosity (h)	5	0.5	2	10	~4
Av. foaming rate (%/h)	4.4	54	20.5	3.2	5.5[b]

[a]A maximum porosity of approximately 40% is mentioned in Refs. 7–9 but without details on temperature, pressure, and time.
[b]Values for core of sandwich structure.

lower bound value for the final pore pressure is p_f = 0.1 MPa (1 atm), Eq. (3) predicts a maximal porosity of 85%. The observed terminal porosities are significantly lower, most probably because of material resistance; as the pores grow, the pressure inside the pores decreases to a level where the deformation rate is negligible and foaming ceases. Additionally, there is a small amount of pore-wall fracture, connecting to the surface of the specimen, creating open porosity. As discussed earlier, ruptured pores are no longer available for further pore expansion.

Using Eq. (3), the pore pressure after foaming exhaustion was determined. Average pore pressures, after reaching maximal porosity, are calculated as 1.9 and 1.7 MPa for foams processed under unbiased isothermal conditions at 903 and 960 °C, respectively. Average pore pressure after unbiased thermal cycling is as low as 0.8 MPa. While the relationship between the pore pressure and the foaming rates is complicated, it is useful to develop a simple approximation to determine the expected change in foaming rates as foaming progresses. Using the creeping pressure vessel model described earlier,[36] a relationship can be developed between the initial foaming rates, $\dot{f}_i$, at high pore pressure and the final foaming rates at low pore pressure, $\dot{f}_f$, assuming no change in deformation mechanism:

$$\frac{\dot{f}_f}{\dot{f}_i} \propto \frac{(p_f)^n}{(p_i)^n} \quad , \tag{4}$$

where n is deformation stress exponent (4.3 for isothermal creep of CP–Ti and 1.0 for TSP during thermal cycling experiments). The "high-pressure" initial condition value is taken to be the HIP pressure, 100 MPa.

Using the above simple approximation, the values of $\dot{f}_f/\dot{f}_i$ calculated from Eq. (4) predict that the foaming rates for the two isothermal cases are expected to drop by almost 8 orders of magnitude from the beginning to the end of foaming, while the thermally cycled foaming rates are expected to drop by about 2 orders of magnitude. This result strongly suggests that the drop in pressure due to pore growth is a major factor in the cessation of foaming and illustrates why TSP leads to larger porosities.

B. Foaming with an external stress

1. Effect of thermal cycling on foaming

As explained earlier, the experimental curves in both Figs. 5(a) and 5(b) would be coincident in the absence of TSP during thermal cycling. However, enhancements in foaming rate, total porosity, and uniaxial elongation are observed under TSP conditions as compared with the isothermal conditions.

The dashed lines in Fig. 5(b) represent the strain rate measured on bulk CP–Ti deformed under TSP conditions with a uniaxial stress of 1 MPa using thermal cycles similar to those in the present study (840–970 °C with a 4-min cycle period[20]). The dotted lines show the expected isothermal creep rate for CP–Ti at 903 °C under uniaxial stress of 1 MPa calculated from data in Ref. 29. After about 6 h of foaming, Fig. 5(b) shows that the average elongation rate of the specimen foamed under cyclic conditions ($1.4 \times 10^{-5}\ s^{-1}$) is the same as that measured on bulk CP–Ti under TSP conditions ($1.1 \times 10^{-5}\ s^{-1}$).[20] This suggests that foaming has ceased, and the titanium foam is simply deforming uniaxially as expected for TSP conditions under a uniaxial stress of 1 MPa. However, at 11.8 h of foaming, the isothermal foam exhibited a strain rate (measured at high temperatures during foaming by load train displacement) of $2.5 \times 10^{-6}\ s^{-1}$, three times higher than the expected rate of $7.3 \times 10^{-7}\ s^{-1}$ for isothermal creep of bulk CP–Ti at 903 °C.[29] It is possible that foaming was not yet completely finished and slow creep expansion of the pores contributed to the measured uniaxial deformation. This hypothesis is supported by the data in Fig. 3, which shows that unbiased, isothermal foaming at 903 °C can continue, albeit at very slow rates, even after 12 h of foaming. Additionally, since the stress exponent of CP–Ti is higher under creeping conditions (n = 4.3) than under thermal cycling conditions where TSP is dominant (n = 1), the isothermal creep rate is more sensitive to the presence of stress concentrations produced by the pores. Such concentrations would enhance the creep rate of the foam in comparison to bulk titanium, at the same effective stress and the same temperature.

From Fig. 6, it is observed that significantly more open porosity is present for the biased thermally cycled case than for the biased isothermally foamed specimen. Total porosity levels are much higher for the TSP case, and thin interpore walls are seen even where pore coalescence is observed [Figs. 7(c) and 7(d)], whereas, in the isothermally foamed specimen, pore coalescence is observed with a lack of thin, interpore regions [Figs. 7(a) and 7(b)] as in the unbiased case above [Fig. 4(b)].

In addition, the biased, thermally cycled specimen exhibited much more open porosity than either unbiased specimen foamed (isothermally at 960 °C or thermally cycled) for 11.8 h (Fig. 6). This observation suggests that the continued uniaxial deformation after foaming cessation, due to the externally applied 1 MPa uniaxial stress, was directly responsible for the increase in open porosity. This is confirmed by density measurements performed on the entire tensile specimen (gauge and heads) after 6 and 10 h of foaming, which show a large increase in open porosity, from an eighth to two-thirds of the total porosity, respectively. The tensile foam specimens had a much larger surface to volume ratio than the cubic specimens foamed without an external load (5 cm^{-1} versus 1 cm^{-1}). The relative number of pores near the surface is, thus, larger for smaller specimens, so more connectivity to the specimen surfaces (and thus more open porosity) is expected.

2. Effect of uniaxial tension of foaming kinetics

Figure 9 presents a comparison of isothermal and cyclic experiments with and without an external biasing stress. As already discussed in detail, thermal cycling induces TSP and thus enhances the foaming rate and terminal porosity over the isothermal foaming in both cases. It is apparent that the foaming kinetics are quite similar (within experimental error) with and without an additional externally applied stress, except after 11.8 h under cycling conditions. This apparent enhancement in foaming with a tensile stress is due to enhanced cavitation at the neck, as discussed earlier. Also, all of the biased TSP foaming data (6 points in Fig. 9) were acquired from a single specimen whereas each of the 9 data points for the unbiased TSP case in Fig. 9 came from a separate specimen. Because terminal porosities and foaming kinetics vary slightly with initial conditions (e.g., variations in the initial porosity due to powder settling in the HIPed billet), it is difficult to discern the true effect of the external biasing uniaxial stress; however, it is apparent from Fig. 9 that this effect is small and of little practical significance.

Finally, as seen by comparing Figs. 4 and 7, the external biasing stress has a strong effect on the pore morphology. The specimen foamed under thermal cycling conditions with the externally applied biasing stress shows elongated pores in the direction of the applied stress, while those foamed without a biasing stress exhibit roughly spherical pores. In particular, the thermally cycled specimen foamed under an external biasing stress showed markedly elongated pores when compared with either the isothermal, biased foams or both thermally cycled or isothermal foams without biasing. Queheillalt *et al.*[13] found pore elongation after rolling and prior to foaming. After foaming, while there were still elongated pores, the pore aspect ratio distribution was found to be tighter than before foaming and the median pore aspect ratio was found to be around 1.0.[13] The ability to tailor pore morphology by simultaneous foaming and deformation has significant practical benefits, for example, in creating foams with elastic anisotropy for various structural and biomedical applications.

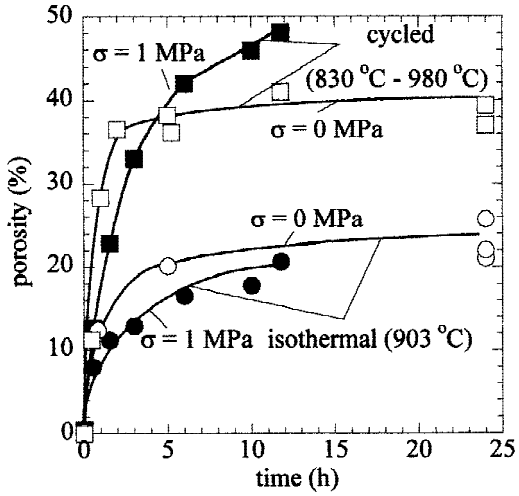

FIG. 9. Porosity as a function of annealing time for isothermal foaming with (solid circles) and without (open circles) an external stress of 1 MPa as well as for foaming under thermal cycling conditions with (solid square) and without (open squares) an external stress. Data are from Figs. 3 and 5(a).

C. Mechanical properties

Figure 8 shows compression behavior similar to what has been reported for numerous other foams or porous solids.[37] A region of linear elasticity is first observed at small stresses and strains. Upon further deformation, a plastic collapse plateau is observed followed by densification demarked by a rapid increase in stress.

Young's moduli for both biased and unbiased isothermal and thermally cycled foams found by compression tests and ultrasonic evaluation are within reasonable agreement, considering the many difficulties in determining Young's modulus from compression data (such as the likelihood of early, undetectable plastic deformation of the cell walls). During ultrasonic evaluation of Young's moduli, only very small strains and stresses are used, causing no permanent deformation, therefore suggesting that the moduli found using this technique are more reliable.

Gibson and Ashby[37] found that the stiffness of open-celled porous materials varies with density as follows:

$$\frac{E}{E_o} = \left(\frac{\rho}{\rho_o}\right)^2 \quad , \tag{5}$$

where E and ρ are Young's modulus and the density of the porous material and where E_o and ρ_o are Young's modulus and the theoretical density of the cell wall material, taken here to be those of bulk titanium (ρ_o = 4.51 g/cm^3, E_o = 110 GPa). While Gibson and Ashby[37] have developed a relation for the relative Young's modulus for closed-cell foams, this relation is more complex, and the data shown in Ref. 37 show that the stiffness of open- and closed-cell foams are very close at the relatively low porosities relevant to the present study. Equation (5) predicts Young's moduli of 67 and 38 GPa for foams with 22% and 41% porosity, respectively. These values are in good agreement with those found by ultrasonic elastic constant evaluation: 60 GPa (22% porosity) and 39 GPa (41% porosity).

Kearns *et al.*[7–9] found that the tensile strength of porous Ti–6Al–4V followed a rule of mixtures up to 32% porosity. Using the rule of mixtures for porous CP–Ti, where the pores are assumed to bear no load, and using 280 MPa as the yield stress for grade II CP–Ti,[38] yield is expected to occur at 220 MPa for a foam with 20–22% porosity and at 160 MPa for 41% porous foam. Yield stresses measured during compression testing were reasonably close to these values (200 and 120 MPa for foams with 20–22% and 41% porosity, respectively).

V. CONCLUSIONS

(1) Solid-state foaming by isothermal creep expansion of high-pressure argon bubbles entrapped by powder HIPing, as first demonstrated by Kearns *et al.*[7–9] in Ti–6Al–4V, was studied for unalloyed CP–Ti at 903 and 960 °C. Foaming rates are significantly faster at the higher temperature, but terminal porosities are equal within error (21–27%). In both cases, pores became spherical after foaming.

(2) Foaming of CP–Ti was also performed by thermal cycling between 830 and 980 °C (straddling the allotropic-temperature), which was expected to activate transformation superplasticity (TSP) as a deformation mechanism. In the present geometry, the volume mismatch between allotropic phases present during thermal cycling about the transformation temperature produces mismatch strains, which are biased by the deviatoric stress from the internal pore pressure. It was indeed demonstrated that thermal cycling leads to (i) accelerated foaming kinetics and (ii) increased maximum attainable porosities, because of the reduced strength and higher ductility of titanium under TSP conditions. Together with an earlier prepublication (Ref. 12), this is the first report of the application of TSP to foaming of metals and to deformation of microscopic features (cell walls) as small as 10 μm.

(3) Foaming of CP–Ti by TSP or by creep with a superimposed externally applied tensile stress does not change terminal porosities or foaming kinetics significantly. However, under TSP conditions it significantly alters the pore morphology and produces pores that are elongated and aligned along the loading axis.

ACKNOWLEDGMENTS

Portions of the work presented in this paper (and published in Ref. 12) were performed at the Department of Materials Science and Engineering of the Massachusetts Institute of Technology, where J.T. was an Exchange Undergraduate Student and D.C.D. received financial support through AMAX in the form of an Endowed Career Development Chair. N.G.D. and C.S. acknowledge the support of the U.S. Department of Defense, through National Defense Science and Engineering Graduate Fellowships.

REFERENCES

1. V. Shapovalov, MRS Bull. **19**(4), 24 (1994).
2. G.J. Davies and S. Zhen, JOM **18,** 1899 (1983).
3. M.J. Donachie, Jr., Adv. Mater. Process. **7,** 63 (1998).
4. M.J. Donachie, Jr., in Titanium and Titanium Alloys Source Book, edited by M.J. Donachie, Jr. (American Society for Metals, Metals Park, OH, 1982), p. 3.
5. S.J. Simske, R.A. Ayers, and T.A. Bateman, Mater. Sci. Forum **250,** 151 (1997).
6. M. Bram, C. Stiller, H.P. Buchkremer, D. Stover, and H. Baur, Adv. Eng. Mater. **2**(4), 196 (2000).
7. M.W. Kearns, P.A. Blenkinsop, A.C. Barber, and T.W. Farthing, Met. Mater. **3**(2), 85 (1987).
8. M.W. Kearns, Formation of Porous Bodies U.S. Patent (IMI Titanium Limited, 1987), U.S. Patent No. 4 659 545.
9. M.W. Kearns, P.A. Blenkinsop, A.C. Barber, and T.W. Farthing, Int. J. Powder Metall. **24**(1), 59 (1988).
10. R.L. Martin, Integral Porous-Core Metal Bodies and in situ Methods of Manufacture Thereof U.S. Patent (McDonnell Douglas Corp., 1996), U.S. Patent No. 5 564 064.
11. D.S. Schwartz, D.S. Shih, R.J. Lederich, R.L. Martin, and D.A. Deuser, in *Porous and Cellular Materials for Structural Applications*, edited by D.S. Schwartz, D.S. Shih, A.G. Evans, and H.N.G. Wadley, (Mater. Res. Soc. Symp. Proc. **521,** Warrendale, PA, 1998), p. 225.
12. D.C. Dunand and J. Teisen, in *Porous and Cellular Materials for Structural Applications*, edited by D.S. Schwartz, D.S. Shih, A.G. Evans, and H.N.G. Wadley, (Mater. Res. Soc. Symp. Proc. **521,** Warrendale, PA, 1998), p. 231.
13. D.T. Queheillalt, B.W. Choi, D.S. Schwartz, and H.N.G. Wadley, Metall. Mater. Trans. **31A**(1), 261 (2000).
14. T.G. Nieh, J. Wadsworth, and O.D. Sherby, Superplasticity in Metals and Ceramics (Cambridge University Press, Cambridge, U.K., 1997).
15. G.W. Greenwood and R.H. Johnson, Proc. R. Soc. London **283A,** 403 (1965).

16. C. Chaix and A. Lasalmonie, Res. Mech. **2,** 241 (1981).
17. D.C. Dunand and C.M. Bedell, Acta Mater. **44**(3), 1063 (1996).
18. N. Furushiro, H. Kuramoto, Y. Takayama, and S. Hori, Trans. ISU **27,** 725 (1987).
19. C. Schuh and D.C. Dunand, Scr. Mater. **40,** 1305 (1999).
20. C. Schuh, W. Zimmer, and D.C. Dunand, in *Creep Behavior of Advanced Materials for the 21st Century,* edited by R.S. Mishra, A.K. Mukherjee, and K.L. Murty (TMS, Warrendale, PA, 1999), p. 61.
21. R. Kot, G. Krause, and V. Weiss, in International Conference on Titanium (Pergamon Press, London, U.K., 1968), p. 597.
22. D.C. Dunand and S. Myojin, Mater. Sci. Eng. **230A,** 25 (1997).
23. D. Leriche, E. Gautier, and A. Simon, in Sixth World Conference on Titanium (Société Française de Métallurgio, Les Ulis Cedex France, 1988), p. 163.
24. C. Schuh and D.C. Dunand, Int. J. Plast. **17,** 317 (2001).
25. C. Schuh and D.C. Dunand, Mater. Sci. Forum **357–359,** 177 (2001).
26. D.C. Dunand, in International Conference on Thermomechanical Processing of Steels and Other Materials (TMS, Warrendale, PA, 1997), p. 1821.
27. J.W. Elmer, J. Wong, and T. Ressler, Metall. Mater. Trans. **29A,** 2761 (1998).
28. W. Szkliniarz and G. Smolka, J. Mater. Proc. Tech. 413 (1995).
29. H.J. Frost and M.F. Ashby, Deformation-Mechanism Maps: The Plasticity and Creep of Metals and Ceramics (Pergamon Press, London, U.K., 1982), p. 44.
30. P. Zwigl and D.C. Dunand, Metall. Mater. Trans. **29A,** 2571 (1998).
31. E.R. Weibel, Stereological Methods; Theoretical Foundations (Harcourt Brace Jovanovich, London, U.K., 1989), p. 140.
32. Material Property Characterization, in Nondestructive Testing Handbook: Ultrasonic Testing, edited by P. McIntire (American Society for Nondestructive Testing, Columbus, OH, 1991), p. 383.
33. R.E. Green, Jr., Introduction to Ultrasonic Testing, in Nondestructive Testing Handbook Ultrasonic Testing, edited by P. McIntire (American Society for Nondestructive Testing, Columbus, OH, 1991), p. 1.
34. E.I. Henneke, Fundamental Principles of Ultrasonic Wave Propagation, in Nondestructive Testing Handbook: Ultrasonic Testing, edited by P. McIntire (American Society for Nondestructive Testing, Columbus, OH, 1991), p. 33.
35. Metals Handbook: Metallography and Microstructures (ASM, Metals Park, OH, 1985), p. 464.
36. L. Finnie and W.R. Heller, Creep of Engineering Materials (McGraw-Hill Book Co., Inc., New York, 1959).
37. L.J. Gibson and M.F. Ashby, Cellular Solids (Cambridge University Press, Cambridge, U.K., 1997).
38. C.A. Kelto, B.A. Kosmal, D. Eylon, and F.H. Froes, in Titanium and Titanium Alloys Source Book, edited by M.J. Donachie, Jr. (American Society for Metals, Metals Park, OH, 1982), p. 280.